Reprinted from Applied Optics, Vol. 25, Page 2955, September 1, 1986

Dependence of speckle size on the laser beam size via photo-induced light scattering in $LiNbO_3$:Fe

Guangyin Zhang, Qing-Xin Li, Ping-Pei Ho, Simin Liu, Zhong Kang Wu and Robert R. Alfano

The dependence of the scattering intensity patterns on the illumination laser beam spot size in $LiNbO_3$:Fe is described. These observations provide direct evidence of the origin of photo-induced light scattering resulting from amplification of scattered radiation caused by imperfections in the crystal.

A coherent laser beam passing through photorefractive crystals [$LiNbO_3$,[1–6] $LiTaO_3$,[7] $SrBaNbO_3$,[8] or $BaTiO_3$ (Ref. 9)] undergoes considerable photo-induced light scattering. It has been postulated that this scattering[5,8] arises from amplification of the weak beam scattered by imperfections in the crystal via the formation of dynamic phase gratings produced by interference of the incident beam with the scattered beams. There has been only indirect evidence to support this proposed mechanism. In this paper we report the observation and give an explanation of the speckle size of the scattering pattern from the illumination beam spot size from photo-induced light scattering in $LiNbO_3$:Fe. Our measurements and theoretical analysis provide direct support for the above-mentioned origin of photo-induced light scattering.

In the experiment, X- or Y-cut thin samples (thickness $t \approx 1$ mm) of $LiNbO_3$:Fe (0.08 wt. %) were positioned perpendicular to the path of a focused 5-mW He–Ne laser (6328-Å) beam. The focal length of the lens was 3 cm. For an extraordinary polarized incident wave, the light was symmetrically scattered with the same polarization over a wide angle, mainly in the plane which included the crystal optic axis and the polarization of the incident beam (Fig. 1). This has been observed by others.[9] Furthermore, we found the features of the light scattering pattern depended on the size of the illumination beam in the crystal.

Photographs of the spatial distribution of scattered light are shown in Fig. 2. The crystal was located at different positions relative to the focal plane. The salient feature shown in these photographs is the dramatic increase in scattering pattern when the crystal is not at the focal spot. In this case, steady-state saturated light scattering was induced over a wide angle with an energy transfer efficiency from incident beam to scattered light of over 80%. When the crystal was moved away from the focal point of the illumination beam, the speckle size was smaller. The energy density of the illumination beam in the crystal was low due to the enlargement of the illumination beam size in the crystal. A comparatively long time (~1 h) was needed to reach the steady-state saturated light scattering pattern. After moving the crystal toward the focal point of the illumination beam, the saturated scattered light intensity became weaker and the scattering cone angle was reduced. When the crystal was located at the exact focal spot of the illumination beam where the illumination beam size in the crystal was very small (a = 12 μm), light scattering did not occur. In this case, the incident beam was defocused during the initial illuminating time for several seconds; it was gradually recovered after a long illumination time.

Using an unfocused beam to illuminate the crystal, the scattering pattern was similar in pattern to that obtained by a focused beam with the same illumination beam size in the crystal. Furthermore, the scattering patterns observed for a focused beam were similar when the crystal was located at equal distance before and after the focal point of the focused beam. These facts indicate that the above-mentioned light scattering pattern mainly depends on the illumination beam size in the crystal and not on the energy density or the curvature of the wave front.

The observation of photo-induced light scattering patterns can be explained as follows. A dynamic phase grating is formed and stored in a crystal by the interference of the incident beam with the beams scattered from the imperfections in a crystal. Due to the

S. Liu and Z. K. Wu are with Nankai University, Physics Department, Tianjin, China; the other authors are with City College of New York, Institute for Ultrafast Spectroscopy & Lasers, New York, New York 10031.

Received 4 December 1985.
0003-6935/86/172955-05$02.00/0.

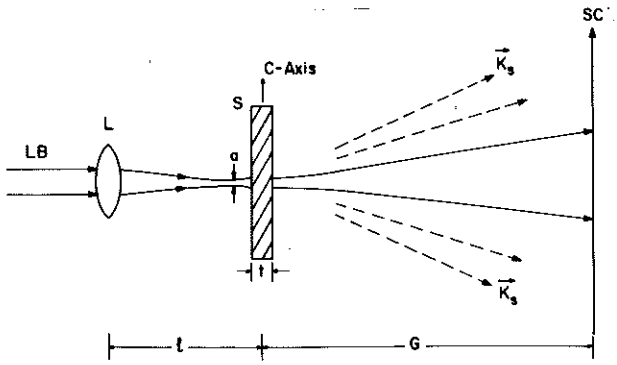

Fig. 1. Experimental setup for the observation of photo-induced light scattering: L, 3-cm focal length lens; S, sample; SC, screen. The distance between lens and screen is 20 cm; the sample is located on a translation stage.

large refractive index of the crystal, the scattered intensity originating from the surface point imperfections should be large. In our model, we propose the formation of the phase grating by interference of the plane incident beam with the spherical scattered wavelets originating from a surface point imperfection on the incident surface of the crystal at the center of the incident beam. This model is displayed in Fig. 3, where $\mathbf{K}_i$ is the wave vector of the plane incident beam and $\mathbf{K}_s^{(1)}$, $\mathbf{K}_s^{(2)}$, $\mathbf{K}_s^{(3)}$, $\mathbf{K}_s^{(4)}$, ... are wave vectors of the spherical scattered wavelets. The recorded phase grating arises from that of different vector components:

$$\mathbf{K}_g^{(1)} = \mathbf{K}_s^{(1)} - \mathbf{K}_i,$$

$$\mathbf{K}_g^{(2)} = \mathbf{K}_s^{(2)} - \mathbf{K}_i,$$

$$\mathbf{K}_g^{(3)} = \mathbf{K}_s^{(3)} - \mathbf{K}_i,$$

$$\mathbf{K}_g^{(4)} = \mathbf{K}_s^{(4)} - \mathbf{K}_i, \ldots .$$

All the vectors terminate on the sphere surface S, which has a radius of $2\pi n/\lambda$, where λ is the wavelength of the beam and n is the refractive index of the crystal. Phase gratings with vector components $\mathbf{K}_g^{(1)}$ and $\mathbf{K}_g^{(2)}$ about $\mathbf{K}_i$ are preferentially induced. This occurs because the scattered beams characterized by these wave vectors [$\mathbf{K}_g^{(1)}$ and $\mathbf{K}_g^{(2)}$] propagate and interact through the longest path in the illumination region of the crystal. Therefore, these wavelets are amplified the most.[10]

From the geometry of phase gratings, we can obtain the values of the vector components $\mathbf{K}_g^{(1)}$ and $\mathbf{K}_g^{(2)}$ (see the Appendix):

$$|\mathbf{K}_g^{(1)}| = |\mathbf{K}_g^{(2)}| = 4\pi(n/\lambda)\sin\{[\tan^{-1}(a/2t)]/2\}, \quad (1)$$

where a is the illumination beam size in the crystal and t is the thickness of the crystal.

In the illumination region, only a few imperfection points are included. The cross-overlapping of fringes of several phase gratings occurs. Therefore, the illumination region within the crystal consists of numerous phase specklons.[11,12] The average size of the specklons can be approximately determined by using the fringe spacing of the phase grating from Eq. (1):

$$2\pi/K = d = [\lambda/(2n)]\{\sin\{[\tan^{-1}(a/2t)]/2\}\}^{-1}. \quad (2)$$

A plot of d as a function of illumination beam size a for $t = 1$ mm and $\lambda = 0.6328$ μm is shown in Fig. 4. It can be seen from Fig. 4(a) that when the illumination beam size in the crystal is <24 μm, the average size of specklons is larger than the illumination beam size in the crystal. This means that the phase grating does not occur in a small illuminated region and that the incident beam cannot induce light scattering. This is the situation when the crystal is located at the focal spot of the light beam.

Experimental values of the average size of phase specklons d, measured from a different beam size a, obtained from the photographs shown in Fig. 2, are plotted in Fig. 4(b). These measured specklon sizes were approximated by the following method: First, the total number of specklons M was counted along the center line of the z axis on the display screen (photographic film). Then assuming that the total number of specklons is the same at the screen and inside the crystal, we estimate specklon size d inside the crystal to be $d = a/M$, where a is the laser beam size at the crystal.

This approximation offers ease of measurement and does not depend on the location of the display screen. The calculated curve from our theoretical model agrees well with our observation. When the crystal was gradually removed from the focal point of the illumination beam, the laser beam size in the crystal became larger and the average size of the phase specklons was reduced. The phase specklon size can be less than the illumination beam size. When the speckle of the scattered light became finer and closer, phase gratings with a larger vector were induced and the wide-angle scattered light was amplified.

Equation (2) can also be derived from the grating equation without using the specklon model. In the conventional approach, the vanishing of induced scattering can be explained when the illumination spot size is less than the induced grating period. The impor-

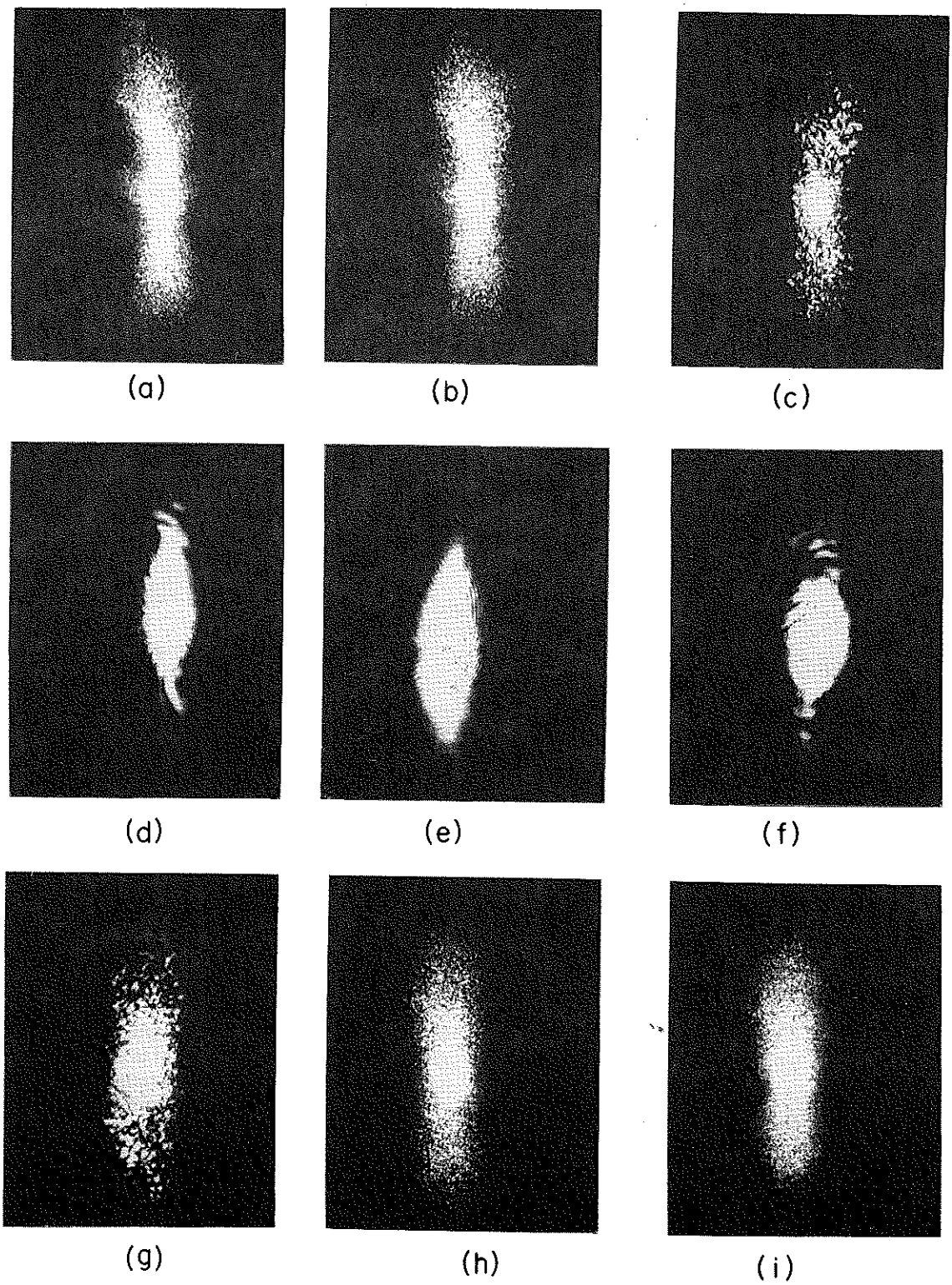

Fig. 2. Photographs of the spatial distribution of scattered light taken for a crystal located at different positions from the focal point of the illumination laser beam: (a) −1.40 cm; (b) −0.90 cm; (c) −0.40 cm; (d) −0.10 cm; (e) 0.xx cm; (f) 0.12 cm; (g) 0.30 cm; (h) 0.80 cm; (i) 1.40 cm; where the corresponding beam sizes are 0.93, 0.60, 0.27, 0.012, 0.08, 0.20, 0.53, and 0.93 mm, respectively. The absolute value of the speckle size depends on the film exposure distance and the magnification factor in the reproduction process.

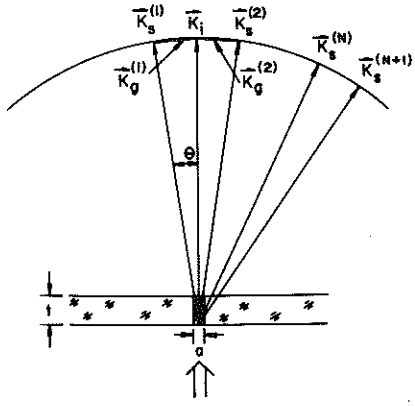

Fig. 3. Schematic representation of the wave vectors of the plane incident beam $\mathbf{K}_i$, the scattered wavelets $\mathbf{K}_s^{(N)}$, and the induced phase grating $\mathbf{K}_g^{(N)}$ originating from a point imperfection on the incident surface of the crystal, where t is the thickness of the crystal.

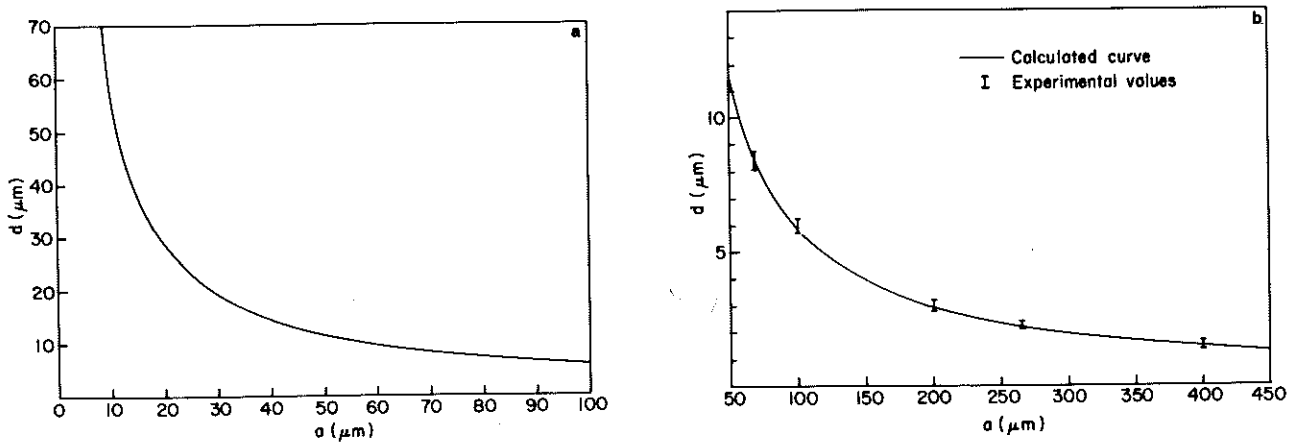

Fig. 4. Average size of specklon d as a function of illumination beam size a in the crystal. The wavelength of the illumination beam is $\lambda = 0.6328$ μm. The thickness of crystal t is 1 mm. (a) Theoretical calculation of Eqs. (2) when $a = 0$–100 μm. (b) A comparison of calculated curve of d with measured values when $a = 50$–450 μm. The solid line is a calculated curve from Eq. (2) to fit the experimental data.

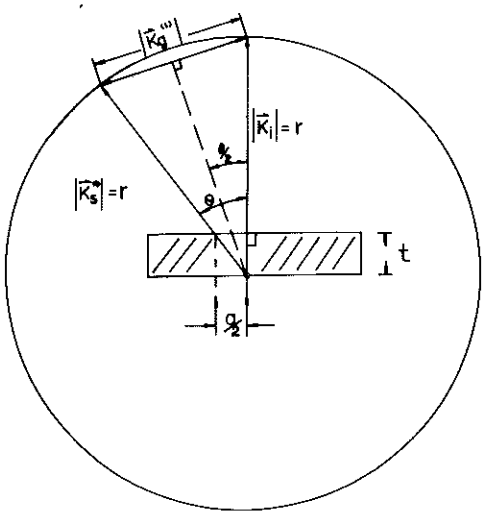

Fig. 5. Geometrical relationship for the derivation of Eq. (1), where $r/2\pi = n/\lambda$ and a is the incident laser beam spot size.

tance of using the specklon model to derive the equation is the simplicity of the interpretation of the induced scattering measurement and in the association of the specklon size with the period of the dominant grating. The specklon size can be measured by a ruler on a projected screen, but measurement of the induced grating period inside a crystal is difficult.

In conclusion, the spatial extension of the laser beam size is important for generation of photo-induced light scattering and for detecting the specklon size. Photo-induced light scattering originates from amplification of the radiation scattered by the imperfections in the crystal.

We wish to thank Robert A. Fisher of Los Alamos National Laboratory for helpful discussions. This research is supported in part by AFOSR, NSF, and PSC/BHE-CUNY.

G. Zhang is an American Physical Society Visiting Senior Scholar from Nankai University, Physics De-

partment, China. Q.-X. Li is a member of the Visiting Scholar Program on leave from Zhongshan University, Physics Department, China.

Appendix: Derivation of Eq. (1)

Using Fig. 5 and trigonometry, we obtain

$$\tan\theta = \frac{a/2}{t}, \tag{A1}$$

$$\mathbf{K}_g = 2r\sin\theta/2 = 2r\sin[\tfrac{1}{2}\tan^{-1}(a/2t)]. \tag{A2}$$

The radius of the sphere in Fig. 5 is

$$r = 2\pi n/\lambda. \tag{A3}$$

Inserting Eqs. (A1) and (A3) into Eq. (A2), we obtain Eq. (1).

References

1. W. Phillips, J. J. Amodei, and D. L. Staebler, "Optical and Holographic Storage Properties of Transition Metal Doped Lithium Niobate," RCA Rev. **33,** 94 (1972).
2. R. Magnusson and T. K. Gaylord, "Laser Scattering Induced Holograms in Lithium Niobate," Appl. Opt. **13,** 1545 (1974).
3. E. M. Avakyan, S. A. Alaverdyan, K. G. Belabaev, V. Kh. Sarkisov, and K. M. Tumanyan, Sov. Phys. Solid State "Characteristics of the Induced Optical Inhomogeneity of $LiNbO_3$ Crystals Doped with Iron Ions," Sov. Phys. Solid State **20,** 1401 (1978).
4. L. F. Kanaev, B. K. Malinovsky, and B. I. Sturman, "Investigation of Photoinduced Scattering in $LiNbO_3$ Crystals," Opt. Commun. **34,** 95 (1980).
5. E. M. Avakyan, K. G. Belabaev, and S. G. Odulov, "Polarization-Anisotropic Light Induced Scattering $LiNbO_3$:Fe Crystals," Sov. Phys. Solid State **25,** 1887 (1983).
6. S. Liu *et al.*, "The Influence of Photo-Induced Refractive Index Change on Raman Spectra of $LiNbO_3$:Fe Crystals," Acta Phys. Sin. **33,** 105 (1984) [Chinese Phys. **4,** 593 (1984)].
7. S. Odoulov, D. Belabaev, and I. Kiseleva, "Degenerate Stimulated Parametric Scattering in $LiTaO_3$," Opt. Lett. **10,** 31 (1985).
8. V. V. Voronov, "Photo-Induced Light Scattering in Cesium-Doped Variant Strotnium Niobate Crystals," Sov. J. Quantum Electron. **10,** 1346 (1980).
9. J. Feinberg, "Asymmetric Self-Defocusing of an Optical Beam from the Photorefractive Effect," J. Opt. Soc. Am. **72,** 46 (1982).
10. B. Ya. Zeldovich, N. F. Pilipetskii, and V. V. Shkunov, "Phase Conjugation in Stimulated Scattering," Sov. Phys. Usp. **25,** 713 (1982).
11. R. Fisher, Ed. *Optical Phase Conjugation* (Academic, New York, 1983), Chap. 6, pp. 137 and 138.
12. In general, the largest amplification of the induced scattering corresponds to the largest value of ΓL, where Γ is the gain coefficient and L is the interaction length. In our experimental arrangement, only L dependence was taken into consideration.